



Micro-vibration monitoring of pipelines using millimetre-wave MIMO radar

Benyamin Hosseiny ^a, Jalal Amini^a and Hossein Aghababaei^b

^aSchool of Surveying and Geospatial Engineering, College of Engineering, University of Tehran, Tehran, Iran;

^bDepartment of Earth Observation Science (EOS), Faculty of Geo-Information Science and Earth Observation (ITC), University of Twente, Enschede, The Netherlands

ABSTRACT

To ensure pipelines' safety it is essential to have a regular and accurate monitoring system to inspect the behaviour of pipelines over time to prevent potential damage. This paper explores the capability of a millimetre-wave multiple-input multiple-output (MIMO) radar system for micro-vibration monitoring of pipelines. Compared to the conventional radars, MIMO radar provides cross-range resolution, while still being capable of monitoring a scene with sub-second data acquisition intervals. This makes it a non-contact system suitable for fast displacement and vibration monitoring. However, the application of MIMO radars has not been fully investigated and analysed for structural monitoring, especially for pipeline vibrations. In this study, a dense time-series of MIMO radar data was collected and processed by proposing a framework based on persistent scatterer interferometry to obtain a map of pipeline vibrations. Experiments were conducted in a controlled environment consisting of both functional and inactive water pipelines. The results showed that the system could detect displacements from micrometre up to sub-millimetre levels, with a displacement error of less than 3 μm . Additionally, the radar could identify the dominant frequencies of 24.375 and 24.500 Hz even in pipelines with very small vibration patterns. These results validate the high potential of millimetre-wave MIMO radar systems for non-contact monitoring of micro-vibrations in pipelines.

ARTICLE HISTORY

Received 12 April 2023



Accepted 27 November 2023

KEYWORDS

vibration; displacement; pipeline monitoring; radar interferometry; persistent scatterer interferometry (PSI)

1. Introduction

Deformation and vibration monitoring are crucial for structural health monitoring (SHM) for early damage detection and improve safety while reducing repair costs. Interferometric processing techniques in radar remote sensing provide valuable insights into structural behaviour and conditions, allowing for non-contact, non-invasive, and non-destructive measurement over extensive areas without causing harm to the structure (Pieraccini 2013). Moreover, radar is insensitive to weather and lighting conditions and capable of penetrating through fog or smoke, thus significantly surpassing optical sensors. Studies in SHM increasingly explore radar remote sensing across various domains,

CONTACT Jalal Amini  jamini@ut.ac.ir  School of Surveying and Geospatial Engineering, College of Engineering, University of Tehran, Tehran, Iran

© 2023 Informa UK Limited, trading as Taylor & Francis Group

including civil structures such as bridges (Michel and Keller 2021) and buildings (Alva et al. 2020), and industrial structures such as pipelines (Monti-Guarnieri et al. 2018).

Pipelines are essential for transporting fluids, including gas, oil, and water, from one location to another. Regular inspections of pipelines help detect potential issues, enabling preventative measures to be taken before significant problems arise (Sampath et al. 2019). Changes in a pipeline's vibration signature, such as an increase in vibration frequency, can indicate damages such as leakage, cracking, or loosened connections (Ghazali, Hee, and Leong 2014; Lalam et al. 2021). Radar technology can provide a continuous monitoring system for detecting deformations and vibrations in multiple areas of a pipeline simultaneously.

Radar can detect vibrations with kilohertz frequencies by sending and receiving thousands of signals per second. However, radar sensing has a primary disadvantage of superposition of targets located in the same radial distance but different cross-range locations, leading to decreased accuracy in displacement measurement and an inability to localize targets in the cross-range direction. Synthetic aperture radar (SAR) addresses this issue by capturing signals from different positions, but the rate of acquiring SAR data is too slow for monitoring vibrations. Multiple input multiple output (MIMO) radar has addressed both of the mentioned limitations (Pieraccini and Miccinesi 2019).

MIMO radar technology employs multiple physical transmitter and receiver antennas to create a larger aperture, in contrast to moving the sensor on a trajectory. This method allows for the precise monitoring of phenomena, with a data acquisition rate of less than a second. MIMO arrays do not require a uniform antenna arrangement, unlike traditional phased arrays. $N_{\text{Rx}} \times N_{\text{Tx}}$ virtual antennas are achievable from the combination of N_{Rx} receiver antennas and N_{Tx} transmitter antennas, making it a popular antenna geometry for MIMO radar systems (Tarchi, Oliveri, and Sammartino 2013). In recent years, many studies have implemented or developed MIMO radar systems for remote sensing-based SHM. However, recent studies have presented the high potential of millimetre-wave automotive MIMO radars for SHM (Baumann-Ouyang et al. 2021; Hosseiny, Amini, and Aghababaei 2023a). By utilizing a W-band signal in MIMO antenna geometry, a compact and lightweight radar system can monitor a short-range area with a sub-second data acquisition rate and moderate cross-range resolution. Consequently, recent studies have explored the potential of these systems for deformation monitoring of bridges, buildings, and wind turbines (Baumann-Ouyang et al. 2023; Miccinesi et al. 2021).

In summary, the safety of pipelines is influenced by various factors, including internal and external forces, as well as time-related degradation such as corrosion and erosion. Therefore, it is crucial to have a regular and accurate monitoring system to inspect the behaviour of pipelines over time and prevent potential damage. While human inspection or a network of contacting sensors such as accelerometers are common approaches for this purpose, they are often expensive and highly inefficient. Radar sensors, on the other hand, are not affected by poor environmental and lighting conditions such as fog, smoke, and poor lighting. Although conventional and MIMO radars possess high potential for structural monitoring, their capabilities and applications are not yet fully investigated in this field, especially for monitoring pipeline vibrations. This paper investigates the capability of millimetre-wave MIMO radar as a non-contact monitoring system that can detect micro vibrations of pipelines. The study area includes a collection of water pipelines that exhibit different vibration and deformation behaviours, with maximum deformation

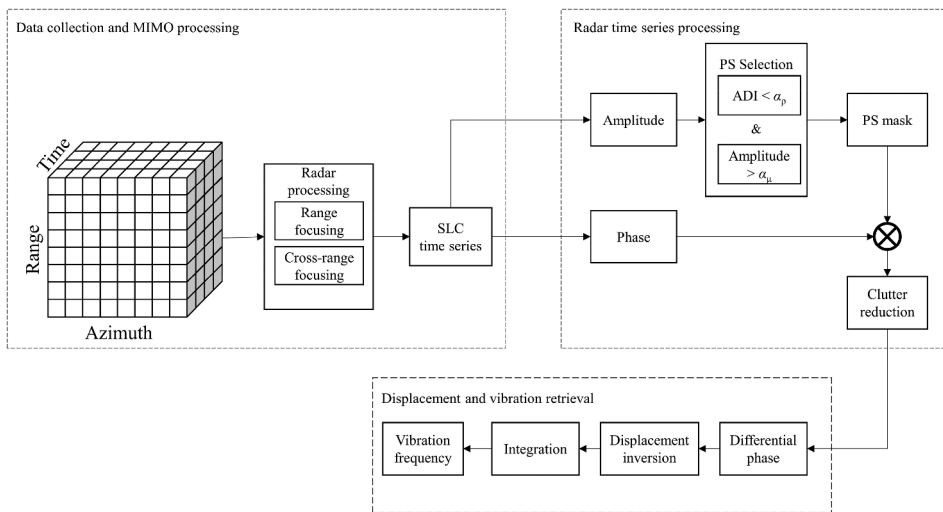


Figure 1. Implemented processing flow to estimate vibration frequencies from time-series of MIMO radar signals.

amplitudes of fewer than a hundred microns. The acquired data consists of a time-series of MIMO radar signals, and deformation and vibrations are obtained through the proposed interferometric processing algorithm. We demonstrate that this monitoring approach is capable of monitoring multiple pipelines, measuring sub-millimetre vibrations, and detecting high vibration frequencies with a millisecond-scale data acquisition interval. Our results showcase the system's ability to detect vibration frequencies of up to 50 Hz.

2. Methodology

This section describes the methodology implemented to monitor pipeline vibrations using MIMO radar data. Figure 1 summarizes the proposed workflow for vibration monitoring using a time-series of MIMO radar data and persistent scatterer (PS) interferometry (PSI) algorithm. Firstly, the data acquisition parameters of the utilized MIMO radar as well as required processing steps are presented. Secondly, we explain the proposed processing flow to detect PS points from the time-series of focused single-look complex (SLC) data. Finally, the differential interferometric processing steps for retrieving displacement signals and vibration frequencies are explained in detail.

2.1. Data collection and MIMO processing

AWR1642BOOST (www.ti.com/product/AWR1642) radar sensor, manufactured by Texas Instruments (TI) is utilized in this experiment. This sensor generates FMCW signal in the frequency range of 76–81 GHz, with maximum bandwidth of 4 GHz. In this study, we have specified a carrier frequency of 77 GHz with a signal bandwidth of 1.5 GHz, resulting in a wavelength of 0.0038 m and a range resolution of 10 cm. Considering that λ denotes signal wavelength, system is composed of 2 Tx antennas with a spacing of 2λ and 4 Rx

antennas linearly separated by a spacing of $\lambda/2$, all operating in vertical polarizations (VV). To increase the number of receivers and consequently improve the angular resolution, we have implemented time division multiplexing (TDM) MIMO processing. This approach involves multiple antennas transmitting in a predetermined time pattern. By doing so, the signals remain distinct despite all antennas transmitting at the same frequency but at different times. As a result, we have achieved 8 virtual receiver elements with a spacing of $\lambda/2$, providing an approximate angular resolution of $\lambda/(8\lambda/2) \approx 14.3^\circ$.

After the receiver antennas collect the backscattered echoes, various techniques such as band-pass filtering and dechirping are used to process the received intermediate frequency signal from the m th virtual antenna of MIMO radar is as follows:

$$s_{if}(m, t) = \exp \left\{ j2\pi \left(f_0\tau + k\tau t - \frac{k\tau^2}{2} + \frac{ml \sin \theta}{\lambda} \right) \right\} \quad (1)$$

where t is the range time, $s_{if}(m, t)$ is the received intermediate frequency signal by the m th antenna, k is chirp slope, f_0 is signal's starting frequency, τ is scattering target's time delay, θ is scattering target's cross-range angle, l is the spacing between the virtual arrays. The focused image is achieved by Fourier transformation (2D-FT) of raw signals in range and cross-range directions. Thus, a complex-valued radar image is obtained in radar's polar coordinate system, where the axes are slant range (R), cross-range angle (θ). In this case, following transformation is required to transform the obtained image into Cartesian coordinate system:

$$\begin{cases} X = R \sin \theta \\ Y = R \cos \theta \end{cases} \quad (2)$$

where (X, Y) is the Cartesian coordinate of a point target located at (R, θ) in the Polar coordinate system.

2.2. Radar time-series processing

In this study, the PSI method is implemented to retrieve displacement signals from MIMO radar observations. To achieve this, a time-series of range-azimuth MIMO radar signals with a zero spatial baseline is collected from the scene of interest. The raw data acquired forms a 3D $N_r \times N_a \times N_q$ matrix, where N_r , N_a , and N_q represent the number of samples in the directions of fast time (range) denoted by r , slow time (azimuth) denoted by a , and repeat time (time) denoted by q . Each pixel of the resulting radar image consists of a complex number comprising the phase and amplitude. The amplitude corresponds to the scattering power of the pixel and can be used to interpret the image scene. Meanwhile, the phase contains range information and is used to measure deformation.

Reliable pixels are chosen based on the amplitude information of the collected time-series of MIMO radar images by generating PS mask using the following criteria:

$$\begin{cases} \mu_A > \alpha_\mu \\ \rho_A = \frac{\sigma_A}{\mu_A} < \alpha_\rho \end{cases} \quad (3)$$

where μ_A and σ_A are a spatial pixel's average amplitude and standard deviation in time; ρ_A is the amplitude dispersion index (ADI), which evaluates pixels' stability during time, and α_μ and α_ρ are the amplitude and ADI thresholds used for filtering the PS points. The

threshold values can be calculated empirically or by automated thresholding algorithms such as Otsu, where the optimum threshold is estimated by the samples' distribution. Finally, unreliable pixels are filtered out by element-wise multiplication of PS mask and the acquired time-series of SLC images.

Due to the low resolution of MIMO radar in cross-range direction, presence of clutters is inevitable, which can affect the final displacement signal. In order to mitigate the impact of static clutter, we employed the circle fitting method on the real-imaginary plot (also known as the phasor plot) of each spatial pixel's time-series. Consequently, the bias caused by the presence of static clutters can be estimated by the central point of the estimated circle. For more details, we refer to the following reference (Hosseiny, Amini, and Aghababaei 2023b).

2.3. Displacement and vibration retrieval

Radar's line of sight (LOS) displacement can be measured based on differential interferometry, which is the phase difference that occurs between two observations at two different times. Therefore, the corresponding LOS displacement of a detected PS pixel is measured in two epochs of t_1 and t_2

$$\Delta R(t_1, t_2) = \frac{\lambda}{4\pi} \Omega(\psi_2 - \psi_1) \quad (4)$$

where $\Delta R(t_1, t_2)$ is the measured displacement between two epochs of t_1 and t_2 , and ψ_1 and ψ_2 are the measured radar phases of the target in the corresponding times. Ω is the wrapping operator that returns the phase value in the range of $[-\pi, \pi]$. Target's displacement at time t_n with respect to the first observation can be achieved by the summation of differential displacements from t_0 to t_n . Thus, a PS pixel's deformation signal in n^{th} epoch of observation is as follows

$$\Delta R(n) = \sum_{i=0}^{n-1} \Delta R(t_i, t_{i+1}) \quad (5)$$

Vibration power spectral density (PSD) P_f of each PS pixel can be estimated by Fourier transform of its deformation signal in time

$$P_f = \text{FT}(\Delta R) \quad (6)$$

According to the Nyquist theorem the maximum detectable frequency is $1/(2\delta_T)$, and the frequency estimation resolution $1/T$, where δ_T and T are data acquisition interval, and total duration of observation, respectively. Thus, shorter data acquisition interval, and longer monitoring time provide higher frequency detection, and better discrimination between the estimated frequencies, respectively.

3. Results and discussion

First, to validate the implemented methodology and initial analysis, numerical simulations were conducted. The radar signal was simulated based on the system parameters mentioned in Section 2.1. Additionally, the system's displacement noise was modelled by a Gaussian distribution with a standard deviation of $2.8 \mu\text{m}$ based on interferometric

processing the time-series signal of a fixed corner reflector. The modelled noise was incorporated into the simulations to provide a more reliable analysis. A point scattering target was then simulated at a distance of 7 m from the radar's LOS, with an azimuth angle of 5° , as demonstrated in Figure 2 (a). Vibrations were simulated using sinusoidal signals, where a simulation of a detected vibration at 25.000 Hz with an amplitude of $10\ \mu\text{m}$ is depicted in Figure 2 (b). For further analysis, we simulated vibrations ranging from 0.5 to 50 Hz frequency and $0.1\text{--}100\ \mu\text{m}$ amplitude. Figure 2 (c) illustrates the relationship between simulated vibrations and the detection signal-to-noise ratio (SNR) in the processed vibration signal. Our findings indicate that signals with lower vibration amplitudes correspond to decreased detection SNR in the vibration PSD. In our studied system, the SNR diminishes when the vibration amplitude reaches near to $1\ \mu\text{m}$. Conversely, no discernible pattern can be observed between the vibration frequency level and the detection SNR. Specifically, for a constant amplitude, the detection SNR remains relatively constant across all frequencies. Notably, Figure 2 (d) shows that only vibration frequencies with high SNR are correctly detected.

Figure 3 shows the investigated area, where the radar sensor covered the specific zone, enclosing the observation of seven cylindrical metallic pipelines with vertical orientation with respect to the radar's looking angle. As identified with blue sign in Figure 3, two of these pipelines were functioning and the water flow was pumping in them. The remaining pipelines were inactive during the experiment. They are labelled with red sign in Figure 3. It is worth noting that these disparate pipelines are connected to each other via the horizontal pipes that are placed near the ceiling. This implies that the vibration of the functioning pipelines could potentially impact the inactive ones, but with lesser power. Also, a fixed 10 cm trihedral metallic corner reflector was placed in the scene for calibration and comparison purposes (shown with white sign in Figure 3).

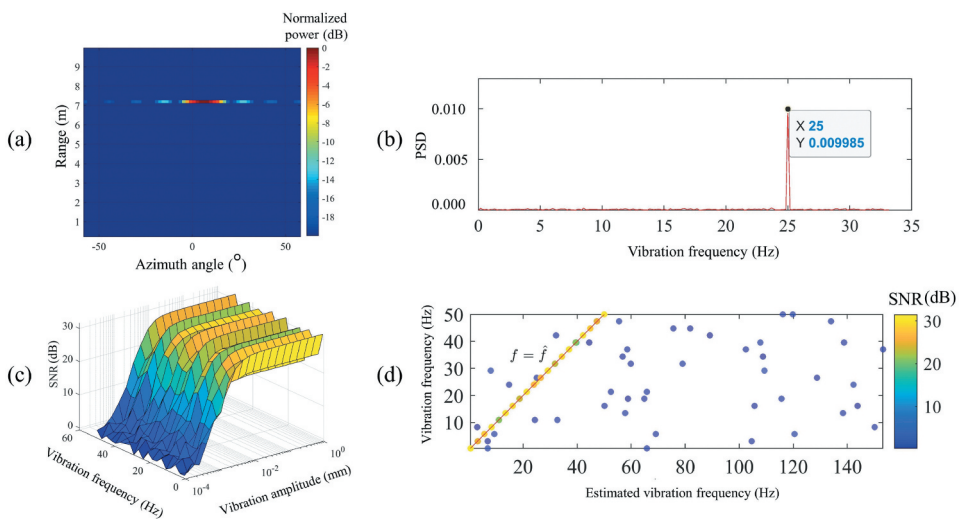


Figure 2. Simulation results: (a) SLC image of point scatterer. (b) Vibration PSD of the scatterer after processing the data. (c) Relation between the vibration frequency, amplitude, and SNR. (d) Estimated vibration frequencies, \hat{f} , against reference frequencies, f .

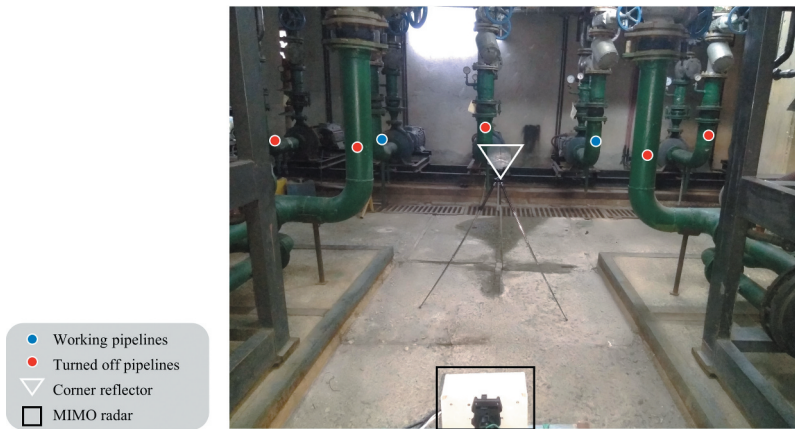


Figure 3. Study area, including the locations of radar sensor and pipelines. The monitored scene comprised of two working and five non-working (turned off) pipelines. Additionally, a fixed corner reflector has been included in the scene for calibration and validation of the measurements.

Eight seconds of time-series data were collected at a 2 ms acquisition interval. To improve SNR and mitigate the impact of noise, the data was accumulated every 4 samples in time, resulting in a data interval of 8 ms. This allows for vibration frequencies reconstruction up to 62.5 Hz, with a resolution of 0.125 Hz. Thus, 1000 MIMO radar images were processed to extract displacement signals and vibration frequencies of the monitored pipelines in the scene. The resulting raw cube data consists of $512 \times 8 \times 1000$ samples in range, azimuth, and time dimensions, respectively. It is worth noting that the acquired size of the data in this study was chosen to manage processing load and demonstrate the feasibility of this approach for micro-vibration monitoring. However, as mentioned in the last paragraph of [Section 3](#), one can acquire longer time-series or a shorter acquisition rate based on project requirements to obtain improved frequency detection resolution or a higher capacity for frequency detection, but at the cost of increased data and processing load.

[Figure 4 \(a\)](#) shows MIMO radar image of the study area. The locations of the existing scattering objects in the scene such as pipelines, wall, water pump, and corner reflector are also depicted for better interpretation.

The MIMO radar's ability to discriminate targets in the azimuth direction is poorer compared to high-resolution SAR imagery, due to the small length of the virtual array (about 14.3° of angular resolution). However, despite this limitation, the radar is still able to detect the location of most pipelines in the azimuth direction. This verifies the usefulness of this type of radar sensor when compared to one-dimensional real aperture radars for pipeline detection applications. The effect of data accumulation (integration) on vibration detection SNR is depicted in [Figure 4 \(b\)](#). As can be noted, the detection SNR has been increased to 23.65 dB after 4 data integration in this study. Notably, the average detection SNR without any integration is 23.27 dB, while after four integrations 0.35 dB is added to the detection SNR (23.65 dB). This indicates the high SNR of results even without integration. Notably, although increasing the integrated data improves the detection SNR, the improvement rate reduces after the third integration.

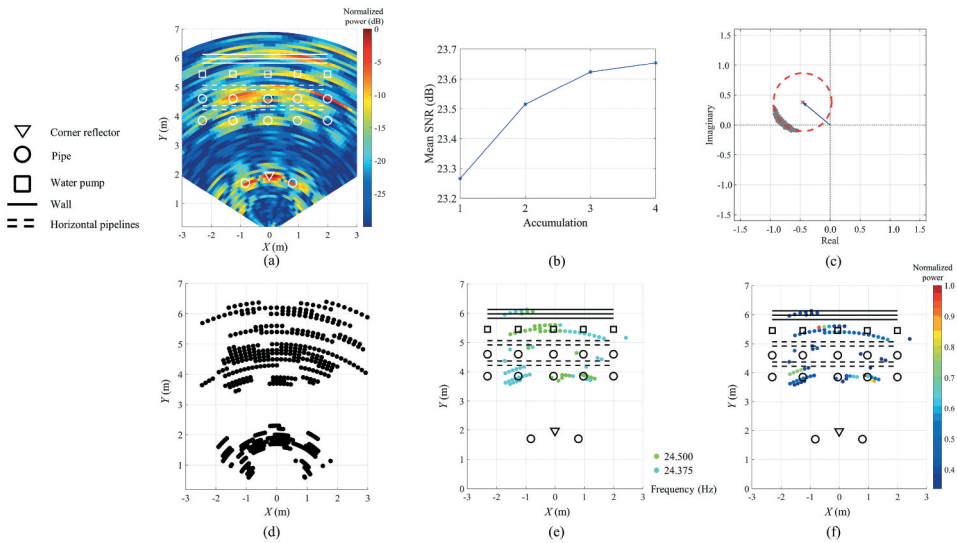


Figure 4. Experimental results: (a) MIMO radar image of the scene. (b) The effect of signal integration on the SNR of vibration detection. (c) An example of the effect of static clutter in one spatial pixel in the phasor plot on complex plane. (d) Detected PS points. (e) Dominant vibration frequency map of vibrating scatterers. (f) Normalized frequency response power at 24.375–24.500 Hz.

PS pixels were chosen based on the condition outlined in Eq. (3). The threshold values for selection were determined through a two-step process. Initially, the Otsu algorithm was employed to estimate the initial values ($\alpha_p = 0.21$, $\alpha_\mu = -16.3$ dB). Subsequently, the final threshold values ($\alpha_p = 0.10$, $\alpha_\mu = -15.0$ dB) were empirically selected to reduce the detection of unnecessary background scatterers. Figure 4 (d) displays the obtained PS mask of the acquired data.

Figure 4 (c) shows how static clutter causes a shift in the distribution of the real and imaginary parts of a moving object during the radar's observation time. The shift vector of each PS point was estimated, and the clutter-removed pixels were then fed into the differential interferometry processing module to retrieve displacement and vibration signals.

After processing the data, each PS point's dominant vibration frequency was extracted and presented in Figure 4 (e). Apart from static scatterers with zero frequencies, two prominent vibration frequencies were detected at 24.375, and 24.500 Hz. As anticipated and evident in this figure, no vibration frequencies were detected in the points corresponding to the corner reflector and inactive pipes (0.0 Hz). However, the processed data revealed 24.375, and 24.500 Hz vibrations for the points that corresponded to the functional pipes. Additionally, according to this figure, some inactive pipes and water pumps exhibited similar vibration behaviour to the functional pipes. This could be due to the fact that, as previously mentioned, these pipelines are interconnected. For example, the pipe located at $X=0.0$, $Y=3.8$ m could be affected by the two functional pipes that surrounded it. Furthermore, water pumps could show similar vibration behaviour because they provide and regulate the power of water flow in the pipes.

For further analysis, [Figure 4 \(e\)](#) illustrates the spectral power of PS points at 24.375 and 24.500 Hz. It can be observed that two functional pipes exhibit the highest power in this frequency, whereas the other pipes in close vicinity demonstrate weaker powers. However, the power around the corresponding pumps remains relatively high. In contrast, the corner reflector and its two adjacent pipes, which are situated far from the functional pipes, exhibit the lowest spectral powers at these frequencies.

In order to provide an in-depth analysis, we extracted displacement signals and PSDs from five different areas in the scene and compared them in [Figure 5](#). The displacement signal for the corner reflector (marked with #2 in the figure) shows a straight line around zero with a standard deviation of 1.46 μm , validating the accurate displacement measurement of the radar system with a noise level of micrometre. Therefore, there are no dominant frequencies evident in the corner reflector's vibration PSD signal. The pipe adjacent to the corner reflector (marked with #2 in the figure) exhibits a similar displacement pattern with a standard deviation of 2.80 μm . Additionally, the resulting PSD displays a faint peak at 24.500 Hz, perhaps as a result of other functional pipes' negligible but detectable (by radar) effect on the pipe.

As anticipated, the displacement signals of the functional pipes (marked with #3 and #5 in the figure) exhibit a higher displacement range with a stronger vibration power. It is noteworthy that the absolute displacement values are below 0.1 mm. Both signals show a peak at 24.500 Hz, with weaker peaks at lower frequencies less than 5 Hz and one peak at 49 Hz. The displacement signal of the inactive pipe surrounded by active pipes (#4 in the figure) depicts more substantial fluctuations than another evaluated inactive pipe. The vibration PSD of this pipe retains a similar pattern with weaker power due to lower fluctuations, caused by external force of active pipes. Among the detected frequencies, the prominent peaks at 24.375 Hz and 24.500 Hz indicate the natural frequencies of the inspected pipes, as they show the strongest responses to the induced forces. However, slightly lower/higher frequencies could be

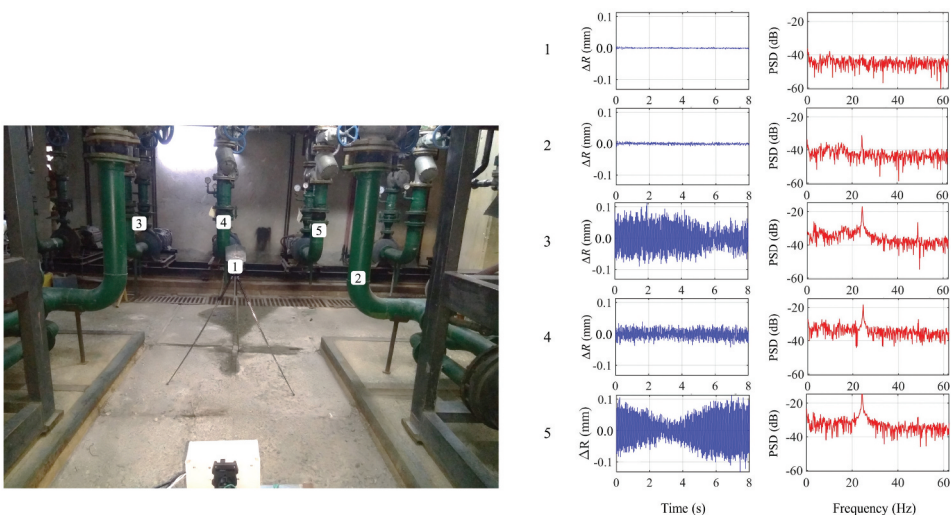


Figure 5. Examples of estimated displacement signal and vibration PSD for different locations (numbered) in the scene.

attributed to damages like corrosions and cracks, which can result in water leaks as observed during inspection (Liu et al. 2020). The peaks observed at 49.000 Hz can be attributed to the effect of harmonics of the main frequencies or excitations caused by the damage and changes in the natural frequency. On the other hand, the presence of lower frequencies can be attributed to factors such as irregular water flow patterns, which are evident in the time-series displacement signals of #3 and #5 (upper graphs in Figure 5) sudden changes in flow velocity, or structural instabilities (Liudmila Victorovna 2018).

The presented results demonstrate the feasibility of millimetre-wave MIMO radars as monitoring systems for micro-vibration monitoring of pipelines. Unlike contact sensors, MIMO radars are non-contact and non-invasive, eliminating the risk of damage to the monitoring object and the monitoring system itself (Li et al. 2015). In comparison to non-contact optical sensors, they are less affected by environmental factors such as dust, dirt, or ambient lighting conditions (Pieraccini 2013). Additionally, MIMO radars can provide subpixel resolution through interferometric processing and operate at a kilohertz rate, unlike vision-based systems. Furthermore, when compared to 1D radar systems, MIMO radars can provide a 2D image with cross-range resolution, resulting in higher spatial coverage (Baumann-Ouyang et al. 2021).

4. Conclusion

Pipelines are susceptible to damage from internal or external forces during usage, necessitating an accurate and continuous monitoring system to prevent potential damages. This study investigated the applicability of millimetre-wave MIMO radar for monitoring micro-vibrations in pipelines. As a non-contact and non-invasive monitoring system, MIMO radar can acquire data from a monitoring scene within milliseconds while providing moderate cross-range resolution. A time-series of AWR1642BOOST MIMO radar data with an acquisition interval of 8 ms was utilized. The study area included several pipelines with diverse functionalities distributed in the radar's illuminated area. The acquired data was processed with a proposed time-series interferometry algorithm for vibration analysis. Results showcase the system's ability to detect vibration frequencies of up to 50 Hz, even with micrometre-scale amplitudes. The utilized sensor could provide a discriminable map of pipelines' location while possessing a moderate cross-range resolution of about 15° by its eight virtual arrays. The obtained results demonstrated the micrometric displacement noise level of the measurements with a standard deviation of 2.8 µm. This means that the experimented system in the frequency band of W is capable of detecting vibrations caused by micrometric displacement patterns. The future studies can be dedicated to the investigation of the vibration monitoring capabilities of MIMO radar on another case studies, and detecting vibration frequencies from high-resolution SAR data.

Disclosure statement

No potential conflict of interest was reported by the author(s).

ORCID

Benyamin Hosseiny  <http://orcid.org/0000-0002-8212-2639>

References

- Alva, R. E., L. G. Pujades, R. González-Drigo, G. Luzi, O. Caselles, and L. A. Pinzón. 2020. "Dynamic Monitoring of a Mid-Rise Building by Real-Aperture Radar Interferometer: Advantages and Limitations." *Remote Sensing* 12 (6): 1025. <https://doi.org/10.3390/rs12061025>.
- Baumann-Ouyang, A., J. A. Butt, D. Salido-Monzú, and A. Wieser. 2021. "MIMO-SAR Interferometric Measurements for Structural Monitoring: Accuracy and Limitations." *Remote Sensing* 2021 13 (21): 4290. <https://doi.org/10.3390/RS13214290>.
- Baumann-Ouyang, A., J. A. Butt, M. Varga, and A. Wieser. 2023. "MIMO-SAR Interferometric Measurements for Wind Turbine Tower Deformation Monitoring." *Energies* 16 (3): 1518. <https://doi.org/10.3390/en16031518>.
- Ghazali, M. H., L. M. Hee, and M. S. Leong. 2014. "Piping vibration due to pressure pulsations." *Advanced Materials Research* 845:350–354. <https://doi.org/10.4028/www.scientific.net/AMR.845.350>.
- Hosseiny, B., J. Amini, and H. Aghababaei. 2023a. "Interferometric Processing of a Developed Mimo Gbsar for Displacement Monitoring." *ISPRS Annals of the Photogrammetry, Remote Sensing & Spatial Information Sciences* 301–306.X-4/W1-202(4/W1-2022). <https://doi.org/10.5194/isprs-annals-x-4-w1-2022-301-2023>.
- Hosseiny, B., J. Amini, and H. Aghababaei. 2023b. "Structural Displacement Monitoring Using Ground-Based Synthetic Aperture Radar." *International Journal of Applied Earth Observation and Geoinformation* 116:103144. <https://doi.org/10.1016/j.jag.2022.103144>.
- Lalam, N., P. Lu, A. Venketeswaran, and M. P. Buric. 2021. "Pipeline Monitoring Using Highly Sensitive Vibration Sensor Based on Fiber Ring Cavity Laser." *Sensors* 21 (6): 2078. <https://doi.org/10.3390/s21062078>.
- Li, C., W. Chen, G. Liu, R. Yan, H. Xu, and Y. Qi. 2015. "A Noncontact FMCW Radar Sensor for Displacement Measurement in Structural Health Monitoring." *Sensors* 15 (4): 7412–7433. <https://doi.org/10.3390/s150407412>.
- Liu, E., X. Wang, W. Zhao, Z. Su, and Q. Chen. 2020. "Analysis and Research on Pipeline Vibration of a Natural Gas Compressor Station and Vibration Reduction Measures." *Energy & Fuels* 35 (1): 479–492. <https://doi.org/10.1021/acs.energyfuels.0c03663>.
- Liudmila Victorovna, M. 2018. "Vibration Strength of Pipelines." In *System of System Failures*, edited by T. Nakamura, Ch. 3. IntechOpen. <https://doi.org/10.5772/intechopen.72794>.
- Miccinesi, L., T. Consumi, A. Beni, and M. Pieraccini. 2021. "W-Band MIMO GB-SAR for Bridge Testing/Monitoring." *Electronics* 10 (18): 2261. <https://doi.org/10.3390/electronics10182261>.
- Michel, C., and S. Keller. 2021. "Advancing Ground-Based Radar Processing for Bridge Infrastructure Monitoring." *Sensors* 21 (6): 2172. <https://doi.org/10.3390/s21062172>.
- Monti-Guarnieri, A., P. Falcone, D. d'Aria, and G. Giunta. 2018. "3D Vibration Estimation from Ground-Based Radar." *Remote Sensing* 10 (11): 1670. <https://doi.org/10.3390/rs10111670>.
- Pieraccini, M. 2013. "Monitoring of Civil Infrastructures by Interferometric Radar: A Review." *Scientific World Journal* 2013. <https://doi.org/10.1155/2013/786961>.
- Pieraccini, M., and L. Miccinesi. 2019. "Ground-Based Radar Interferometry: A Bibliographic Review." *Remote Sensing* 11 (9): 1029. <https://doi.org/10.3390/rs11091029>.
- SamPATH, S., B. Bhattacharya, P. Aryan, and H. Sohn. 2019. "A Real-Time, Non-Contact Method for In-Line Inspection of Oil and Gas Pipelines Using Optical Sensor Array." *Sensors* 19 (16): 3615. <https://doi.org/10.3390/s19163615>.
- Tarchi, D., F. Oliveri, and P. F. Sarmartino. 2013. "MIMO Radar and Ground-Based SAR Imaging Systems: Equivalent Approaches for Remote Sensing." *IEEE Transactions on Geoscience and Remote Sensing* 51 (1): 425–435. <https://doi.org/10.1109/TGRS.2012.2199120>.